390285-2-T

# A Uniform Physical Optics Approximation for Scattering by S-Shaped Surfaces

J.L. Volakis, L.C. Kempel, and T.B.A. Senior

November 1990

Northrop Corporation
8900 E. Washington Blvd.
Pico Rivera, CA 90660-3737

# A Uniform Physical Optics Approximation for Scattering by S-shaped Surfaces

J.L. Volakis, L.C. Kempel, and T.B.A. Senior

November 1990

**Abstract**

When an S-shaped surface posseses no derivative discontinuities, techniques such as the Geometrical Theory of Diffraction are not applicable. However, if the radius of curvature is relatively large at every point on the surface, the physical optics approach may be employed. In this report, we present a Uniform Physical Optics (UPO) solution. The UPO solution remains valid at caustic regions associated with the merging specular points approaching from either side of the inflection point of the S-shaped surface. It is developed by approximating the surface with a localized cubic expansion leading to exact expressions in terms of Airy functions. In contrast to other solutions, the one given here requires only knowledge of the stationary phase points and the first two derivatives of the surface generating function at those points. The validation of the developed P.O. solution is presented in a companion report and based on results included in that report, recommendations are outlined here for future improvements in the available theoretical predictions of the scattering by S-shape surfaces.

# 1 Introduction

Of interest in this study is a characterization of the scattering by a class of smooth surfaces possessing an inflection point at which the radius of curvature is infinite (see Fig. 1). This belongs to a special class of convex-concave surfaces and recently several asymptotic studies have appeared in the literature for an evaluation of the scattering by these surfaces. As can be expected, these studies have concentrated on the evaluation of the scattering in the nonspecular or shadowed region[1, 2] which is characterized as the region with no geometrical optics returns. Of particular concern has also been the development of a uniform solution which remains valid in the transition region (i.e. the region near the shadow boundary separating the specular and nonspecular regions), and recently Pathak and Liang [3] presented such a solution that overcomes the limitations of earlier uniform solutions [4, 5, 6]. All these asymptotic solutions are based on a physical optics approximation of the surface current distribution and the aforementioned papers have only been directed at the evaluation of the physical optics integral.

In the next section a simple uniform evaluation of the physical optics integral is presented which parallels that given in [3] but avoids the introduction of the numerous geometrical parameters appearing in that solution. The solution provided by UPO will be compared to an evaluation by the stationary phase method. The final section will summarize this UPO formulation as well as discuss its merits and anticipated region of applicability.

# 2 Uniform Physical Optics Approximation

## 2.1 H-polarization

Consider the two-dimensional S-shaped surface, shown in Fig. 1, described by a function $y = f(x)$ with $f''(0) = 0$. The surface is illuminated by the plane wave

$$\mathbf{H}^i = \hat{z} e^{jk_o(x\cos\phi_o + y\sin\phi_o)} \tag{1}$$

giving rise to the scattered field

$$\mathbf{H}^s = -\frac{j}{4}\int_C \mathbf{J}(\overline{\rho}') \times \nabla \left[H_o^{(2)}(k_o|\overline{\rho} - \overline{\rho}'|\right] d\ell' \tag{2}$$

where $C$ describes the surface contour in the $xy$ plane, $k_o$ is the free space propagation constant, $H_o^{(2)}(\cdot)$ is the zeroth order Hankel function of the second kind and $\mathbf{J}(\overline{\rho})$ is the induced surface current. As usual, $\overline{\rho}' = x'\hat{x} + y'\hat{y}$ denotes the integration point and $\overline{\rho} = x\hat{x} + y\hat{y} = \rho(\hat{x}\cos\phi + \hat{y}\sin\phi)$ is the observation point. For far zone observations, of primary interest here, we allow $\rho$ to approach infinity and (2) then simplifies to

$$\mathbf{H}^s \simeq -\frac{1}{2}\sqrt{\frac{k_o}{2\pi}}\,\frac{e^{-j(k\rho-\pi/4)}}{\sqrt{\rho}}\int_C [\hat{\rho}\times\mathbf{J}(\overline{\rho}')]\,e^{jk_o(x'\cos\phi+y'\sin\phi)}d\ell' \tag{3}$$

where it remains to specify or find the surface current density $\mathbf{J}(\overline{\rho})$. On the basis of the physical optics approximation we set $\mathbf{J}(\overline{\rho}) = \mathbf{J}_{po}(\overline{\rho}) = 2\hat{n}\times\mathbf{H}^i$, with $\hat{n}$ being the upward unit normal to the surface $y = f(x)$. Substituting for

$$\hat{n} = \frac{\hat{y} - \hat{x}f'(x)}{\sqrt{1+(f'(x))^2}} \tag{4}$$

and noting that

$$d\ell = \sqrt{1+(f'(x))^2}dx \tag{5}$$

(3) reduces to

$$\mathbf{H}^s \approx -\hat{z}\sqrt{\frac{k_o}{2\pi}}\,\frac{e^{-j(k_o\rho-\pi/4)}}{\sqrt{\rho}}\int_{-\infty}^{\infty}[f'(x')\cos\phi - \sin\phi]\,e^{jk_o[Cx'+Sf(x')]}dx' \tag{6}$$

in which

$$S = \sin\phi + \sin\phi_o \tag{7a}$$

and

$$C = \cos\phi + \cos\phi_o \tag{7b}$$

A non-uniform expression for the far zone scattered field is now readily obtained by evaluating the integral via the stationary phase method. This yields

$$\begin{aligned}\mathbf{H}^s \;\sim\; & -\hat{z}\frac{e^{-j[k_o\rho-\pi/4]}}{\sqrt{\rho}}\sum_{i=1,2}\sqrt{\frac{1}{S|f''(x_{si})|}}\,e^{-j\frac{1}{2}arg\{f''(x_{si})\}} \\ & \cdot\,[f'(x_{si})\cos\phi - \sin\phi]\,e^{jk_o[x_{si}C+f'(x_{si})S]}\end{aligned} \tag{8}$$

where $x_{si}$ denote the two stationary phase points found from a solution of the equation

$$f'(x_{si}) = -\frac{C}{S} = -\frac{\cos\phi + \cos\phi_o}{\sin\phi + \sin\phi_o}\bigg|_{\phi=\phi_o} = -\cot\phi_o \tag{9}$$

The stationary phase points $x_{si}$ specify the specular points of the surface, whose location depends on the angles of incidence and observation. For an odd function $f(x)$, $x_{s1} = -x_{s2}$, and we observe that for $0 < \pi - \phi_o < \frac{\pi}{2}$, as $\pi - \phi$ decreases the specular points disappear. First, as $\pi - \phi$ decreases the two stationary points coalesce to zero and since $f''(0) = 0$, (8) becomes invalid. The $\phi$ angle at which this occurs is the shadow boundary (see fig. 1) and for lower $\pi - \phi$ angles (shadowed region) there are no reflected fields as defined in the classical geometrical optics sense. In the shadowed region the stationary points specified by (9) become imaginary and the evaluation of the integral in (6) must then be performed via the steepest descent method. Nevertheless, in [1, 2, 3] the stationary phase method was still used in the standard manner except that the contribution of the stationary point having negative imaginary part was discarded because it results in a wave violating the radiation condition. Based on this, the scattered field in the shadowed or non-specular region is asymptotically given by

$$\mathbf{H}^s \sim -\hat{z}\frac{e^{-j(k_o\rho-\pi/4)}}{\sqrt{\rho}}\,\frac{f'(x_{si})\cos\phi - \sin\phi}{\sqrt{S|f''(x_{si})|}}\,e^{-j\frac{1}{2}arg\{f''(x_{si})\}}e^{jk_o[Cx_{si}+Sf(x_{si})]} \tag{10}$$

on the assumption that $Im(x_{si}) > 0$. It can be shown that this result is identical to that obtained via the steepest descent method.

To derive an expression for the scattered field which remains valid for observations near the shadow boundary (transition region) we return to the PO integral in (6). Since $x_{si}$ is small in the transition region, the odd function $f(x)$ may be replaced by the first two terms of the Maclaurin series expansion, i.e.

$$f(x) \simeq f'(0)x + \frac{f'''(0)}{6}\,x^3\,. \tag{11}$$

When this is introduced into (6) and the non-exponential portion of the

integrand is replaced by its value at the saddle point we find

$$\mathbf{H}^s \approx +\hat{z}\sqrt{\frac{k_o}{2\pi}}\,\frac{e^{-j(k\rho-\pi/4)}}{\sqrt{\rho}}\left(\frac{C}{S}\cos\phi+\sin\phi\right)\int_{-\infty}^{\infty}e^{j(\alpha x^3-\beta x)}dx \tag{12}$$

with

$$\alpha=\frac{k_o f'''(0)S}{6} \tag{13a}$$

and

$$\beta=-k_o\left[C+f'(0)S\right]=0 \tag{13b}$$

Noting now the identity

$$\pi(3\alpha)^{-1/3}Ai\left\{\pm(3\alpha)^{-1/3}\beta\right\}=\int_0^{\infty}\cos(\alpha x^3\pm\beta x)dx=\frac{1}{2}\int_{-\infty}^{\infty}e^{j(\alpha x^3\pm\beta x)}dx \tag{14}$$

we obtain

$$\begin{aligned}\mathbf{H}^s &\sim \hat{z}\frac{e^{-j(k\rho-\pi/4)}}{\sqrt{\rho}}\sqrt{2\pi k_o}\left(\frac{C}{S}\cos\phi+\sin\phi\right)(3\alpha)^{-1/3}Ai\left\{-(3\alpha)^{-1/3}\beta\right\}\\ &\sim \hat{z}\frac{e^{-j(k\rho-\pi/4)}}{\sqrt{\rho}}\sqrt{2\pi k_o}\left(\frac{1+cos\phi cos\phi_o+sin\phi sin\phi_o}{\sin\phi sin\phi_o}\right)(3\alpha)^{-1/3}Ai\left\{-(3\alpha)^{-1/3}\beta\right\}\end{aligned} \tag{15}$$

where $Ai(\cdot)$ is the tabulated Airy function of complex argument.

It is clear that because of (11), expression (15) is valid only in the transition region and in fact it does not reduce uniformly to the results given in (8) and (10) for observations in the deep specular or non-specular regions. To ensure this, it is necessary to employ a more accurate expansion for the odd function $f(x)$. In view of the aforementioned uniformity requirements we expand $f(x)$ as

$$f(x)S=(C-\beta)x+\alpha x^3 \tag{16}$$

with

$$\alpha=-\frac{\left[k_o S f''(x_{si})\right]^2}{12\beta} \tag{17a}$$

and

$$\beta = \begin{cases} \frac{1}{2}\sqrt{-3k_o^2 Sf''(x_{si})\left[Cx_{si} + Sf(x_{si})\right]} & \text{specular region} \\ -\frac{e^{j\frac{\pi}{4}}}{2}\sqrt{-3k_o^2 Sf''(x_{si})\left[Cx_{si} + Sf(x_{si})\right]} & \text{non-specular region} \end{cases} \tag{17b}$$

in which $Re(x_{si}) \geq 0$ and $Im(x_{si}) \geq 0$. When (16) is introduced into the exponential portion of the integrand in (6), the result is again (15) with $\alpha$ and $\beta$ as given by (17). For these values of $\alpha$ and $\beta$, (15) reduces uniformly to (8) or (10) when in the deep specular or non-specular regions, respectively, in addition to being valid in the transition region (for $x_{si} \to 0$, the $\alpha$ and $\beta$ values given in (17) reduce to those in (13)). To show that (15) in conjuction with (17) reduces to (8) and (10) we must introduce the large argument asymptotic representations of the Airy function [7]

$$Ai(-z) \sim \frac{1}{2\sqrt{\pi}} z^{-1/4}\left[e^{j\left(\frac{2}{3}z^{3/2}-\frac{\pi}{4}\right)} + je^{-j\left(\frac{2}{3}z^{3/2}+\frac{\pi}{4}\right)}\right] \tag{18}$$

in the deep specular region and

$$Ai(z) \sim \frac{1}{2\sqrt{\pi}} z^{-1/4} e^{-\frac{2}{3}z^{3/2}} \tag{19}$$

in the deep non-specular region. The asymptotic result given by (15) is, therefore, valid everywhere with $\alpha$ and $\beta$ as defined in (17). We remark that this result is also comparable to the leading term given in (23) and (31) of [3], but is written here in a much more simplified form.

## 2.2 E-polarization

Let us now assume that the S-shape surface is illuminated by the plane wave

$$\mathbf{E}^i = \hat{z} e^{jk_o(x\cos\phi_o + y\sin\phi_o)} \tag{20}$$

The far zone scattered field is then given by

$$\mathbf{E}^s = \frac{Z_o}{2}\sqrt{\frac{k_o}{2\pi}}\,\frac{e^{-j(k_o\rho-\pi/4)}}{\sqrt{\rho}} \int_C \left[\hat{\rho}\times\hat{\rho}\times\mathbf{J}(\overline{\rho}')\right] e^{jk_o[x'\cos\phi + y'\sin\phi]} d\ell' \tag{21}$$

where $Z_o$ is the free space intrinsic impedance. When $\mathbf{J}(\overline{\rho}')$ is again approximated by $2\hat{n}\times\mathbf{H}^i = 2\hat{n}\times\hat{\rho}^i\times\mathbf{E}^i/Z_o$, with $\hat{\rho}^i = -(\hat{x}\cos\phi_o + \hat{y}\sin\phi_o)$ denoting the direction of incidence,we have

$$\mathbf{E}^s = \hat{z}\sqrt{\frac{k_o}{2\pi}}\,\frac{e^{-j(k_o\rho-\pi/4)}}{\sqrt{\rho}}\int_{-\infty}^{\infty}[f'(x)\cos\phi_o - \sin\phi_o]\,e^{jk_o[Cx'+Sf(x')]}dx' \quad (22)$$

with $S$ and $C$ defined in (7). We observe that apart from the interchange of $\phi$ and $\phi_o$ in the non-expenontial portion of the integrand and a change of sign, (22) and (6) are identical and thus a uniform asymptotic expression for the E-polarization scattered field is

$$\begin{aligned}\mathbf{E}^s &\sim -\hat{z}\frac{e^{-j(k_o\rho-\pi/4)}}{\sqrt{\rho}}\sqrt{2\pi k_o}\left(\frac{C}{S}\cos\phi_o + \sin\phi_o\right)(3\alpha)^{-1/3}Ai\left\{-(3\alpha)^{-1/3}\beta\right\}\\ &\sim -\hat{z}\frac{e^{-j(k_o\rho-\pi/4)}}{\sqrt{\rho}}\sqrt{2\pi k_o}\left(\frac{1+cos\phi cos\phi_o + sin\phi sin\phi_o}{\sin\phi sin\phi_o}\right)(3\alpha)^{-1/3}Ai\left\{-(3\alpha)^{-1/3}\beta\right\}\end{aligned} \quad (23)$$

The parameters $\alpha$ and $\beta$ are again given by (17) and we remark that the E and H polarization expressions are identical for all angles except for a change in sign.

# 3 Example Computations

In this section we present examples where the UPO solution is employed to compute the scattering by a few S-shaped surfaces. This UPO solution is compared to the usual non-uniform one based on the standard stationary phase method.

The S-shape surfaces to be examined here are of the form

$$y = f(x) = A\,erf(cx) = \frac{2}{\sqrt{\pi}}A\int_0^{cx} e^{-t^2}dt. \quad (24)$$

i.e, the surface is described by a scaled error function with the $A$ and $c$ constants providing some control on the slope and height of the S-shape surface. It is seen that for large $x$, $f(x) \approx \pm A$, depending on whether x is positive or negative. Thus, the height of the S-shaped surface as described

by (24) is approximately $2A$ whereas the value of $c$ provides a control on the slope of the S-curve at the inflection point(see example curves in Fig. 2) It is important to note that the S-shape curves obtained from (24) do not contain any surface discontinuities and although this may not be true in practice, it is essential for this preliminary study in assessing the effectiveness of the UPO solution.

Figure 3 compares the uniform and non-uniform backscatter patterns for a surface generated by (24) when A = -0.1 and c = 6 at 5 GHz (As noted earlier the E and H polarization patterns are identical.). It is seen, that the agreement is quite good with the exception of the caustic region where $f''(x) \approx 0$. Similar agreement is observed in Figure 4 where we compare bistatic patterns corresponding to $\phi_o = 60$ degrees for the same surface. In all patterns, the UPO solution smoothly reduces to the stationary phase solution when away from the shadow boundary.

# 4 Concluding Remarks

In this study, we presented a Uniform Physical Optics solution for scattering by S-shaped surfaces. The accuracy of this solution was examined in a companion report [8] where it was shown to be in good agreement with numerically generated data provided no whispering gallery mode effects are present. It should be noted that the S-shaped surfaces examined in this respect were continuously differentiable and must also be odd about the inflection point. This is necessary for agreement between the numerical and physical optics solutions for backscatter calculations near grazing. As demonstrated in [8] the low echowidth observed in figures 3 and 4 for small $\pi - \phi$ occurs in spite of the presence of high surface currents near the inflection point. This implies that contributions from the surface currents on either side of the inflection point generate cancelling effects. It was observed, however, that the cancellation of these contributions can be easily disturbed when using, for example, non-uniform sampling which results in artificially generated returns unless the numerical discretization and associated current expansion are based on higher order approximations. The numerical simulation employed in [8] was unfortunately based on a pulse-basis expansion of the current and furthermore the S-shaped surface was discretized in flat segments causing additional approximations in the simulation.

Although the above modelling approximations can be alleviated by ensuring that uniform sampling is employed for the discretization of the S-shaped curve, this is not the case when surface discontinuities are present. For arbitrarily located surface discontinuities, it is necessary to resort to non-uniform sampling and unless higher order modelling of the surface and the current is employed, the numerical results will not be of acceptable accuracy. This is illustrated in Figure 5, where we compare the scattering patterns for the same error function when discretized with uniform and non-uniform sampling. In the case of non-uniform sampling , the surface was subdivided into twenty small segments and each of these was discretized with different sampling. It is clear from Figure 5, that substantial difference exists between the backscatter patterns in the non-specular region.

To permit an accurate evaluation of the scattering (possibly non-PO) by arbitrary S-shaped surfaces, one approach is to reformulate the integral equation solution by introducing higher order basis and surface elements. This will ensure continuity of the currents from one zone to another (i.e. charges at the breakpoints between two segments are eliminated) resulting in a more accurate prediction of the true surface current. The implementation of this model is certainly a non-trivial task and it is recommended that it be pursued as a followup task.

# References


[1] H. Ikuno and L.B. Felson. Real and complex rays for scattering from a target with inflection points. *Radio Sci.*, 20(2):952–958, Nov. 1987.

[2] H. Ikuno and L.B. Felson. Complex ray interpretation of reflection from concave- complex surfaces. *IEEE Trans. Antennas Propagat.*, 36:1260–1271, Sept. 1988.

[3] P.H. Pathak and M.C. Liang. On a uniform asymptotic solution valid across smooth caustics of rays reflected by smoothly indented boundaries. *IEEE Trans. Antennas Propagat.*, 38:1192–1203, Aug. 1990.

[4] N.C. Albertsen, P. Balling, and N.E. Jensen. Caustics and caustic corrections to the field diffracted by a curved edge. *IEEE Trans. Antennas Propagat.*, 35:297–303, May 1977.

[5] Y.A. Kravtsov. A modification of the geometrical optics method. *Radiofizika*, 7:664–673, 1964.

[6] D. Ludwig. Uniform asymptotic expansion at a caustic. *Commun. Pure Appl. Math.*, XIX:215–250, 1966.

[7] J. Heading. *An Introduction to Phase-Integral Methods*, John Wiley and Sons, New York, 1972.

[8] L.C. Kempel and J.L. Volakis. Numerical Simulation of the Scattering by S-shaped Surfaces. University of Michigan Radiation Laboratory Tech Report 390285-1-T, Nov. 1990.

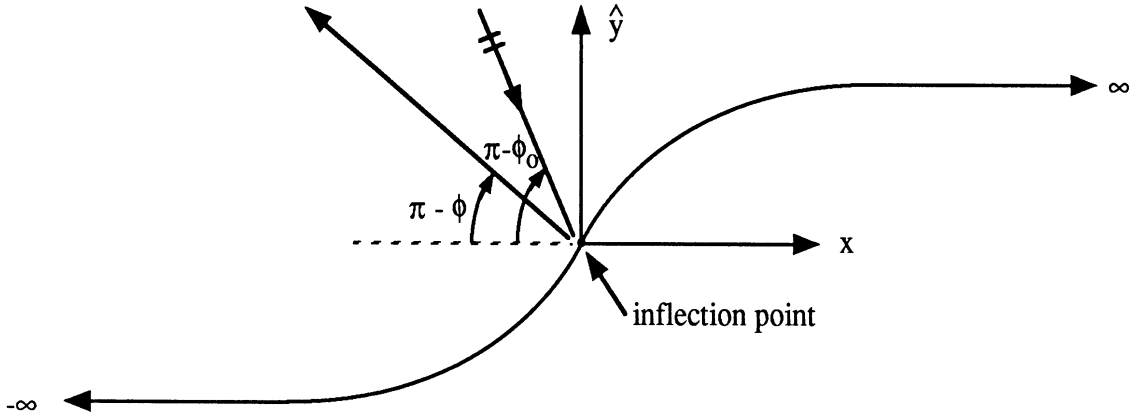


Fig. 1a. Geometry of the S-shape surface.

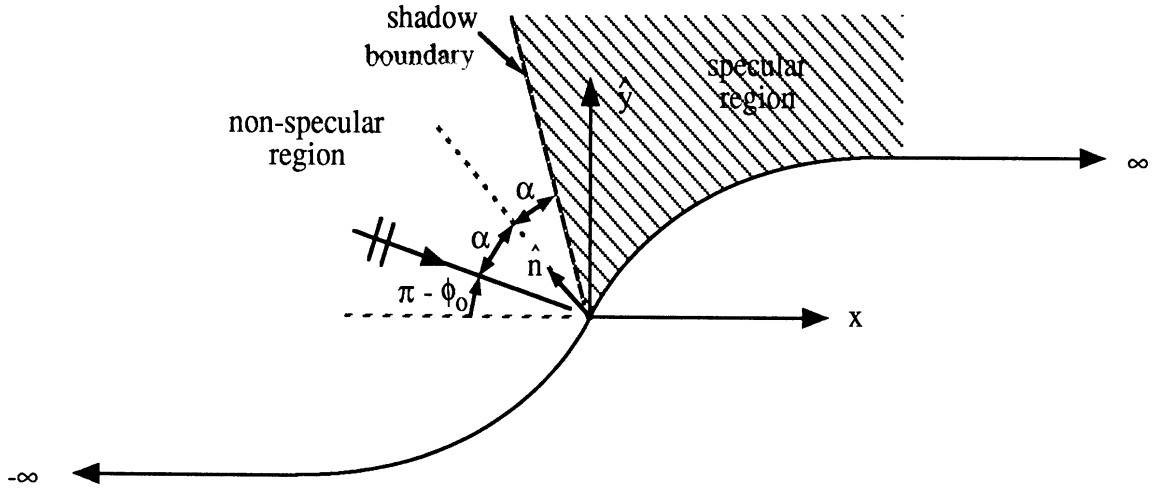


Fig. 1b. Definition of the shadow boundary.

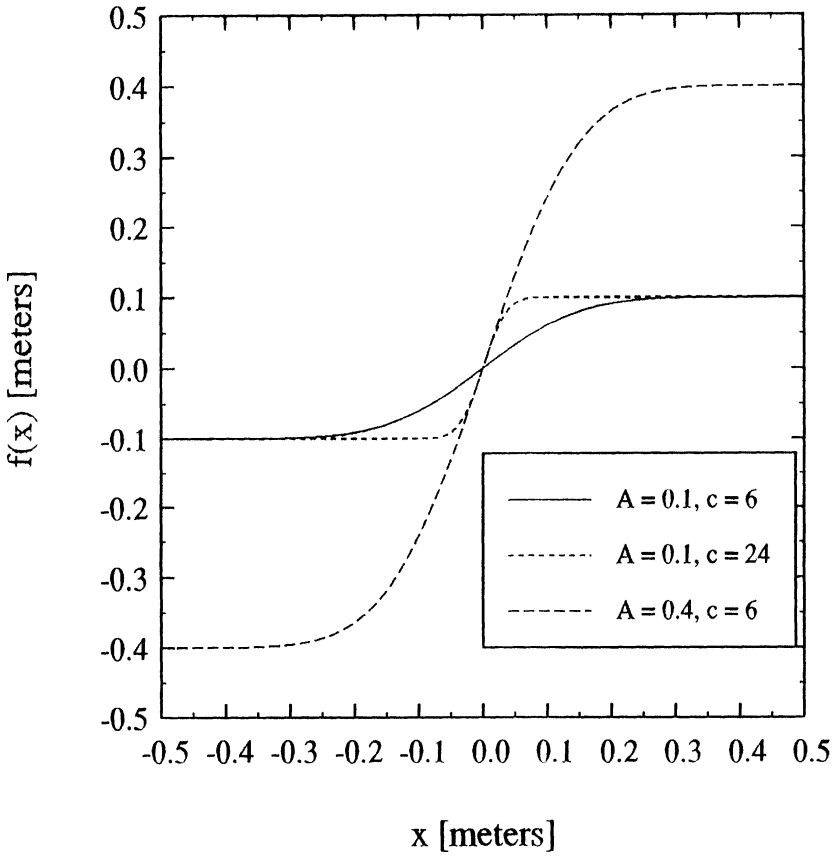


Figure 2. Typical curves for different A and c values in the error function of equation 24.

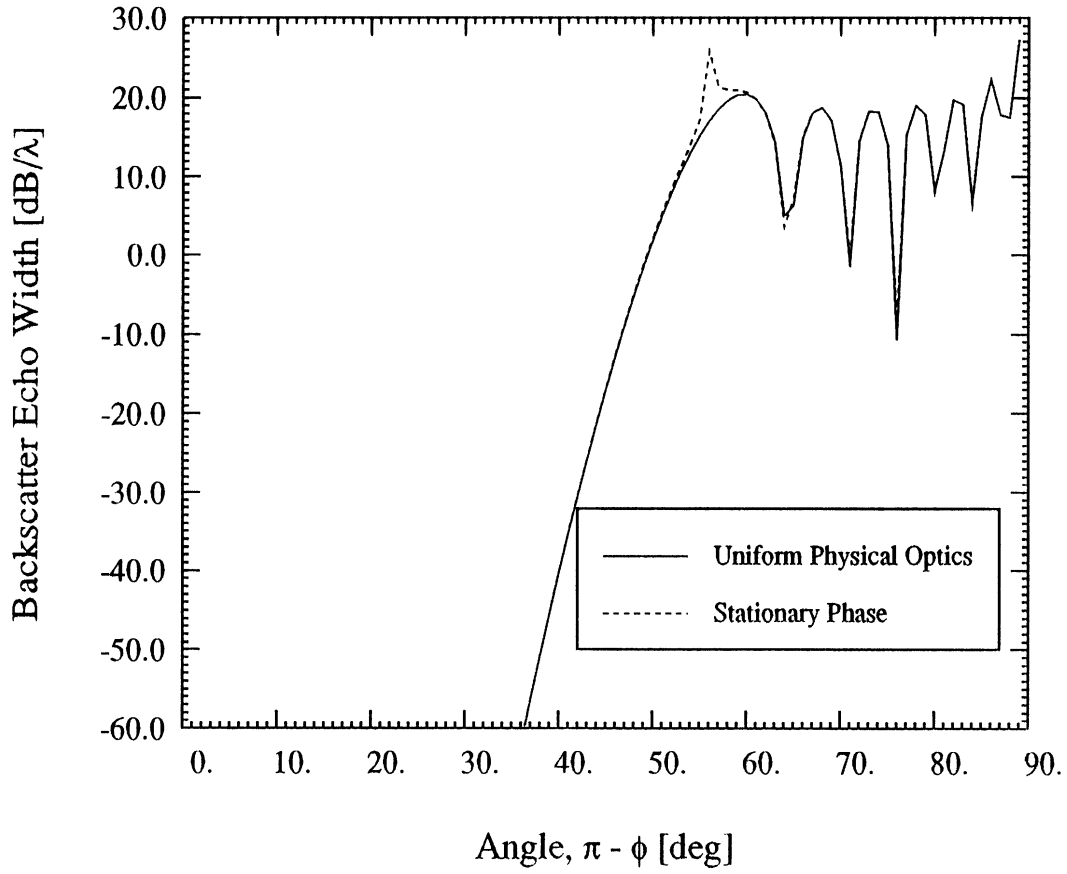


Figure 3. Comparison of UPO vs. Stationary Phase backscatter patterns for a surface generated by (24) when A = -0.1 and c = 6 at 5 GHz.

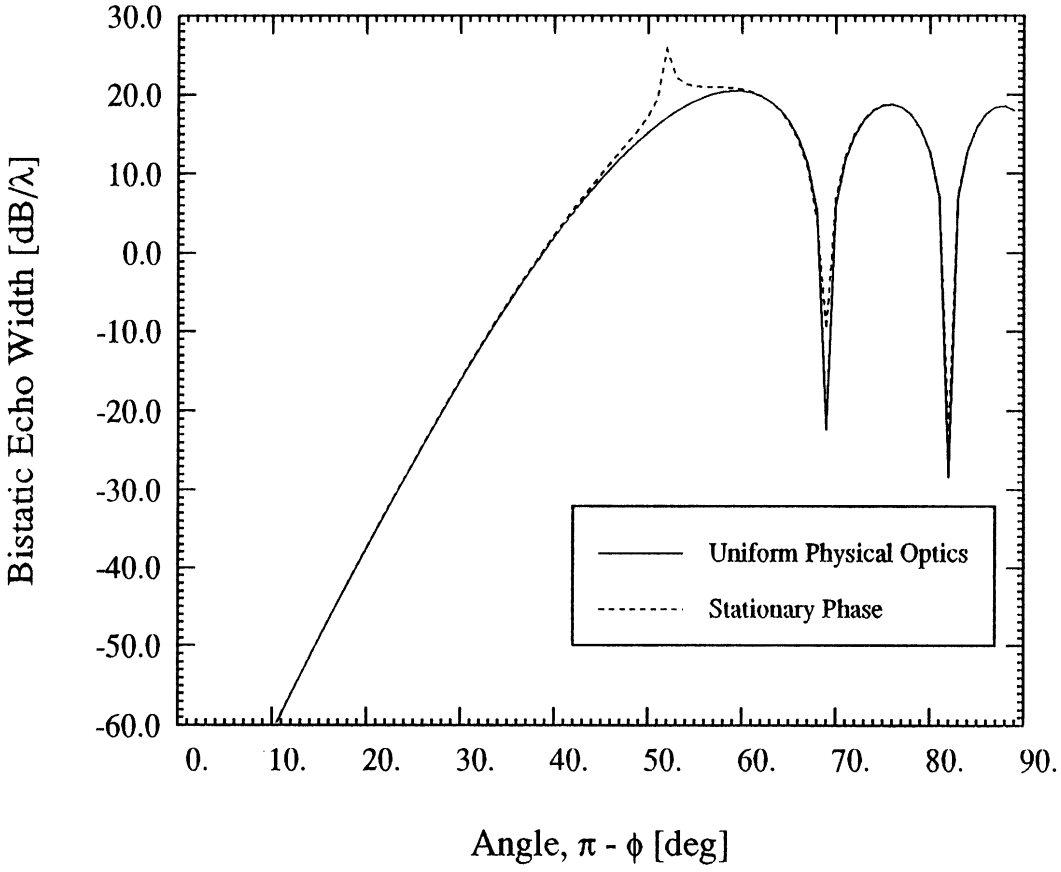


Figure 4. Comparison of UPO vs. Stationary Phase bistatic patterns with an incidence at 60 degrees for a surface generated by (24) when A = -0.1 and c = 5 GHz.

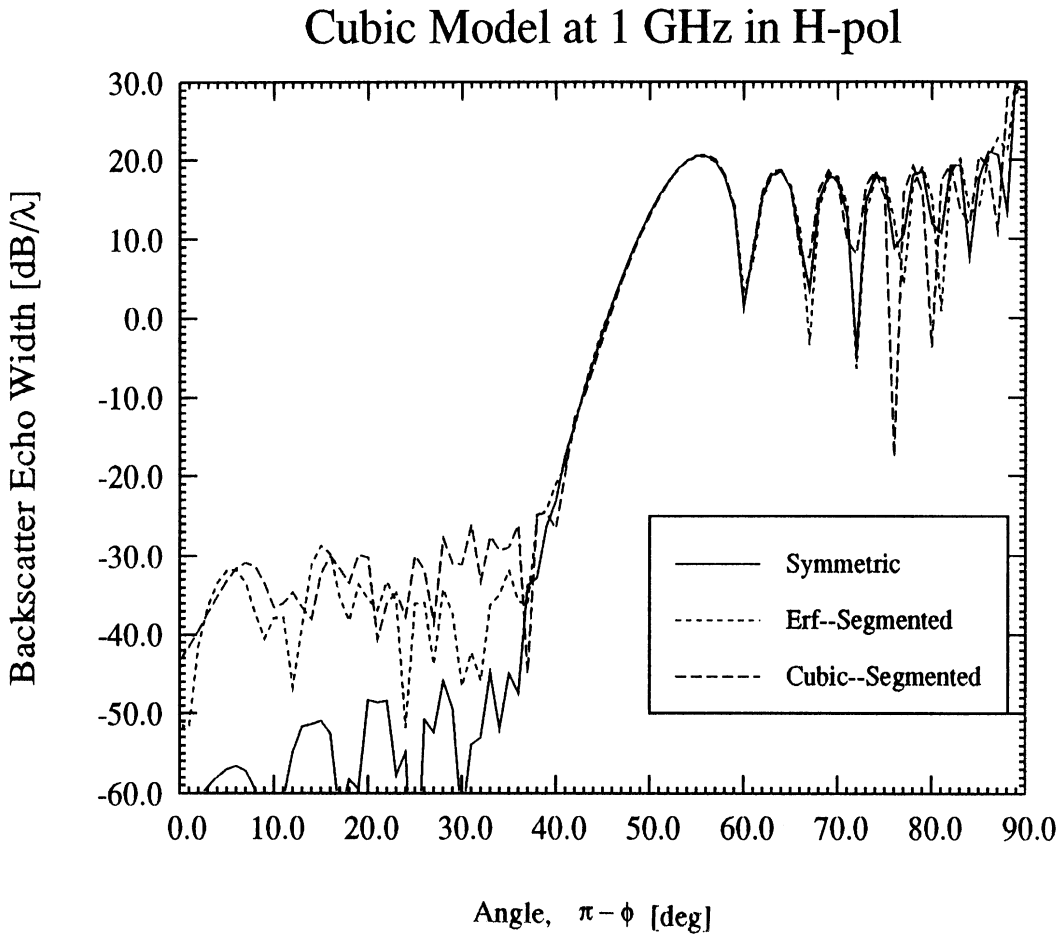


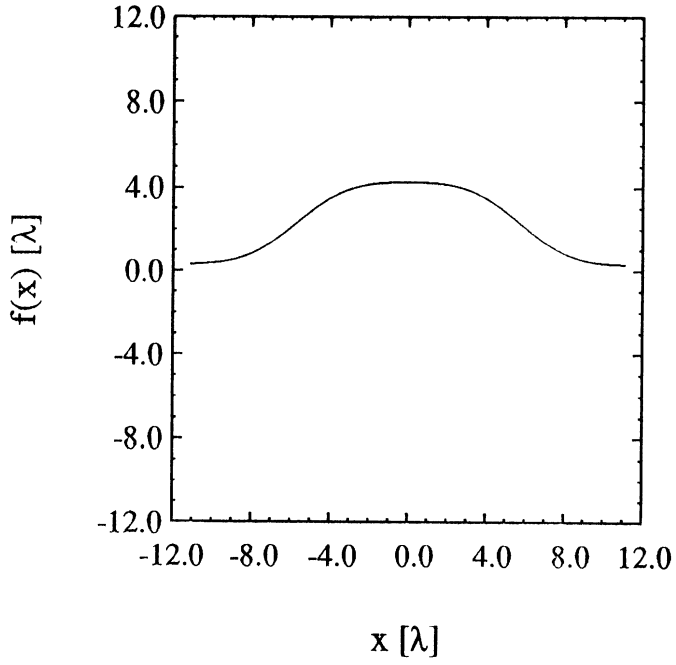


Figure 5. Comparison of backscatter patterns (for the surface shown) using uniform and non-uniform sampling.